Applied Thermal Engineering 127 (2017) 46–57

Contents lists available at ScienceDirect

Applied Thermal Engineering

journal homepage: www.elsevier.com/locate/apthermeng

Research Paper

Fabrication and testing of CONTISOL: A new receiver-reactor for day and night solar thermochemistry

Justin L. Lapp, Matthias Lange, René Rieping, Lamark de Oliveira, Martin Roeb *, Christian Sattler

German Aerospace Center, Cologne, Germany

HIGHLIGHTS

- First view of a new concept combining solar chemistry and solar thermal storage.
- Target temperatures for methane reforming (850 °C) were reached in testing.
- Thermal qualification is done using D-optimal design of experiments procedure.
- SiSiC monolith was unsatisfactory and will be replaced by an Inconel version.

ARTICLE INFO

Article history:
Received 28 October 2016
Revised 28 July 2017
Accepted 1 August 2017
Available online 2 August 2017

ABSTRACT

The CONTISOL concept is a new vision of an integrated solar receiver/reactor for a variety of thermochemical processes. The concept includes a single monolithic solar absorber with two inter-mixed, but non-intersecting sets of gas channels. One set of channels is always used for a chemical process. During daytime operation, the other set of channels is used to heat air which is sent to thermal storage. During nighttime operation, the air flow is reversed, transferring heat from thermal storage to the monolith through the same set of channels, thus providing energy to continue chemical processing continuously through day and night. In this paper we introduce the general operation of the system and discuss its benefits applied to solar methane reforming as an example process. Past solar reactors which influenced the development of CONTISOL are discussed. A 5 kW scale demonstration prototype has been constructed at DLR and thermal experiments have been conducted using the DLR high flux solar simulator. A statistical design-of-experiments procedure has been applied to evaluate the influence of absorber temperature, gas flow rates, and gas inlet temperatures on heat transfer rates to gas streams, and to construct a thermal performance map of the device. The target gas outlet temperatures of over 850 °C were reached during these tests. Limitations on the initial design of the monolith are discussed including recommendations for future improvements.

1. Introduction

Solar thermal energy is a promising source of process heat for a variety of thermochemical processes, from splitting water to produce hydrogen, to upgrading of carbonaceous feedstocks [1], to providing process heat for CO_2 capture. The benefits are a nearly limitless supply of available energy and high quality heat that, given only sufficient optics, can reach temperatures of over 2000 °C. The concept of concentrating solar energy for fuel production addresses some major limitations of solar energy, specifically the harnessing of low flux energy for high-temperature processes, and the ability to transport energy from locations with plentiful sunlight to those with less. However, many concepts still deal with issues of transients. The most impactful transient is the day-night cycle. This leads to most solar reactor systems being shut down at night until sunlight is available the next day. Solar energy systems must also deal with smaller scale transients like the gradual increase and decrease of irradiation during the day, and sudden, significant changes in irradiation due to cloud passing. Most directly irradiated solar thermochemical systems must deal with these transients by varying the production rate and they possibly have a change in product mixture or quality due to changing temperature. Solar thermal storage can address transients, but usually add several energy conversion steps between the solar radiation and the chemical reaction.

A new concept is proposed here that addresses many of the challenges related to transients for directly irradiated solar thermochemical reactors. We have developed this concept as a general solar thermochemical reactor which can be used to operate a num-

* Corresponding author.
E-mail addresses: Justin.Lapp@dlr.de (J.L. Lapp), Martin.Roeb@dlr.de (M. Roeb).

http://dx.doi.org/10.1016/j.applthermaleng.2017.08.001
1359-4311/

Nomenclature

$\dot{Q}$	power (W)
t	time (s)
T	temperature (°C)
$\dot{V}$	volumetric flow rate (l min^{-1})
x	horizontal position from monolith axis (m)
y	vertical position from monolith axis (m)
z	axial position in monolith (m)

Subscripts

front	face of the monolith facing the solar input
side	gas channels entering and exiting on the sides of the monolith
str	gas channels entering and exiting on the ends of the monolith

ber of processes. However, for the current demonstration, we consider solar reforming of methane as the example process. Before describing the concept in detail, we present a brief background on solar methane reforming, as many of the reactor concept developments in this field influenced the new concept presented in this work, and it is one of the most direct applications that can benefit from its advancements.

2. Background on solar methane reforming

Currently, largest source of hydrogen is production by steam-methane reforming using natural gas feedstock [2]. Though promising long term solutions to removing the fossil fuel feedstocks from hydrogen production are under study, many of these solutions have long horizons until economic feasibility is expected. Significant reductions in environmental impact can be obtained by implementing intermediate solutions, which do not remove the fossil fuel feedstocks, but deploy improvements to the current reformation processes to improve output. One such option for upgrading the fuels is a conversion of the currently common steam-methane reformation process to use solar energy.

The reforming reaction which converts methane (CH_4) and steam (H_2O) to CO and hydrogen (collectively synthesis gas or syngas)

$$CH_4 + H_2O \rightarrow CO + 3H_2 \quad (1)$$

is endothermic, requiring a significant heat source at temperatures over 800 °C, as well as a catalyst. Typically, the energy for the endothermic reaction is produced by combusting a portion of the feedstock, yielding a syngas output with 70% of the energy content of the feedstock [3]. If solar energy is harnessed to supply the heat necessary for the reaction, no feedstock is consumed and the output has 20% more energy than the feedstock [4]. Solar steam reforming leads to 71% more syngas produced compared to traditional reforming given the same amount fossil fuel input. Additionally, dry reforming is an option to convert methane to higher energy fuels using CO_2 instead of steam

$$CH_4 + CO_2 \rightarrow 2CO + 2H_2 \quad (2)$$

The products of Eqs. (1) and (2) can be directly used as an energy carrier, or they can be further processed. Mixed reforming, accomplished by reacting methane with a mixture of steam and CO_2 can be used to control the ratio of CO and H_2 in the product stream, in order to deliver ideal mixtures for downstream processes like Fischer-Tropsch conversion of syngas to liquid fuels like gasoline and diesel fuel [5].

Solar methane reforming dates back to thermodynamic analysis and experiments in the early 1980's by Chubb of the U.S. Naval Research Laboratory [6]. Experimental campaigns have been completed from laboratory scale to on-sun industrial-scale (100's of kW) demonstrations with high conversion rates of up to 70% [7–9]. These experimental campaigns have showed that solar methane reforming is a feasible technology with a high probability of success, and made it an ideal choice to demonstrate our concept. A complete review of solar methane reforming technologies can be found in Agrafiotis et al. [10].

Most solar methane reformation reactors can be divided into one of two categories – indirectly heated or directly heated. Indirectly heated concepts rely on absorption of solar radiation on one surface and transfer through an intermediate medium to the chemical reaction site. Tubular receiver concepts are common, relying on radiation absorption on the outside of a tube and conduction through the tube wall to provide energy for the reaction in the tube. Initial studies by Chubb [6] and by the Institute of Catalysis, Novosibirsk [11] were both indirect concepts that used tubes heated by solar radiation from the outside and containing a catalyst and the reactant flow on the inside. Scaled up catalyst-packed-tube concepts have been operated at up to 200 kW by CSIRO [12,13], and up to 480 kW by the Weizmann Institute (WIS) [14]. Indirect concepts can also use a heat carrier to transfer absorbed solar energy to a separate device for reforming. The ASTERIX project, a joint project between CIEMAT and DLR, used air heated by a solar tower to drive a separate steam reformer operating at 170 kW of thermal power [15]. The WIS, in cooperation with Sandia National Laboratories (SNL), demonstrated a receiver/reactor utilizing vaporization and condensation of sodium for heat transport between concentrated sunlight and a catalytic packed bed for methane reforming [16,17]. All indirect concepts provide the advantage of eliminating a window, allowing easier operation of the reaction at high pressures, and generally are constructed from simple components like catalyst filled tubes. Later concepts utilizing heat carriers allow receiver and reactor device designs and operation to be decoupled, provide the potential for intermediate energy storage, and have less variation due to the solar input.

Direct heat transfer devices are characterized by the chemical reactants having access to surfaces that are directly irradiated by solar energy. Though this generally increases design complexity, in particular by requiring a window to allow irradiation to enter sealed areas of the reactor, it allows for higher theoretical process efficiency and a smaller overall system. The first such system tested was the CEASAR reactor joint project between DLR and SNL. A windowed chamber contained catalyst coated α-alumina-mullite foam through which reactants flowed [7]. Subsequent projects by DLR and WIS scaled up the concept, with the foam structures forming a domed cavity, to 300 kW [18] and 400 kW [19] levels. A similar design using a metal foam has also been tested by Inha University of Korea [20]. The WIS has also taken an alternative approach to high surface area for reactions, in the "porcupine" directly irradiated solar reformer, with catalyst coated on closely-spaced alumina pins [21]. The preceding concepts have utilized foams or pins to provide high surface area for both heat transfer and catalyst coating. We have incorporated this feature in our concept with a structured honeycomb.

While the current work focuses on flexibility as a means to high efficiency, some recent works have sought efficiency through higher conversion or faster reaction rates. Extreme temperatures are a means to high conversion rates without the necessity of catalysts, but at the expense of solar collection efficiency [7]. The use of molten salts to enhance heat transfer and allow for limited energy storage is another recent area with significant focus [22]. The molten salt has been proven to mitigate temperature variations during short solar transients but has not been proven for nightly energy storage for reforming applications. In addition, it presents challenges to reactor design and plant operation.

Heating air to store solar energy is another maturing technology. Going back to heating of rock beds by passing air through the bed, solar energy has been stored in various materials to circumvent the natural disadvantage of solar energy: transients due to cloud cover and the day night cycles. Open volumetric receivers are commonly used to heat air by solar energy, by passing the air through a solar absorbing inert material [23]. To allow for energy storage, the air typically transfers energy to a storage medium, and the reverse operation can be used to remove energy from the medium.

3. Our concept

The goal of the new concept, shown in Fig. 1, is to combine the high efficiency and fast response of directly irradiated solar reactors with the flexibility and continuous product stream of indirect systems with thermal storage. The concept uses a monolithic volumetric solar absorber with two sets of channels that are separated from each other. One set of channels is used for thermochemical processing. The inner surface of the channels provides a suitable surface with high area to hold a catalyst, as needed for methane reforming or a variety of other thermochemical processes. Most ceramic construction materials are naturally suited for adhering a catalyst by slurry coating, while metal and finer ceramics are suitable after acid etching. The other set of channels is used to heat air. A large surface area of the channels and thin walls provide good heat transfer between the two gas streams.

This concept has several advantages over typical solar thermochemical reactors, including direct or indirect methane reforming reactors discussed above. First, the air stream provides a direct adjustment of capacity of the gas flows to take up the solar energy input, without necessitating a variation in chemical production rate. Therefore, this reactor can theoretically produce a constant stream of products during times of varied solar input, like cloud passing, sunrise, and sunset. Second, compared to some energy carrier designs like air or molten salt systems, the transfer of solar energy to the reactants is more direct, leading to lower losses and allowing the system to begin production earlier during heat-up. Also, compared to molten salt or other high heat transfer fluids, reactor design and material selection are much simpler because of the ease of handling the air stream relative to a molten salt system. In fact, the design of the air handling system is no more complicated than the methane and product handling system. Third, the transfer of energy to air allows for storage of energy in high efficiency storage systems like latent heat or thermochemical storage. Several suitable options exist at the temperatures necessary for methane reforming. For example, latent heat storage in copper or copper alloys, which melt between 900 and 1100 °C, or thermochemical storage in cobalt oxide, which reacts at 900 °C. Fourth, the flow of the air stream can be reversed, transferring energy from the storage back to the reactor, allowing the thermochemical process to operate exclusively from stored energy for nighttime operation. Finally, the flexibility of the design allows for multiple modes of operation with one system, such as one to produce a constant stream of products and another to maximize daily total production. Energy transferred to a storage system will be subject to some level of losses, leading to lower solar-to-fuel efficiency for stored energy compared to energy absorbed in the reaction channels. It will be up to future plant designers to weigh these energy losses with the benefits of a continuous product stream and twenty-four hour operation. Not all processes will benefit from these factors. For those that do, the CONTISOL concept presents a potential efficiency improvement compared to indirect systems where all of the energy passes through a storage system.

Though the current prototype is designed to be demonstrated with methane reforming, the concept is flexible to be used with many thermochemical processes, including those that require catalysts and those that do not. The advantages of high surface heat transfer area, controllable energy update rate, and nighttime operation are advantageous to many solar processes.

Fig. 2 shows schematics of daytime and nighttime operation of the receiver-reactor. During the day the chemical reaction takes place and air is heated by the monolith to be sent to thermal storage. A closed loop for the air stream means that air must only be heated from the lowest storage temperature, just below the reaction temperature. At night, air is pumped through the thermal storage to carry energy from storage to the receiver-reactor, where this energy powers the chemical reaction. During shorter transients like cloud passing, sunrise, and sunset, the receiver-reactor could be operated in daytime mode but with lowered flow rate of air to keep the flow rate of reactants constant, or it could even temporarily be switched to nighttime mode.

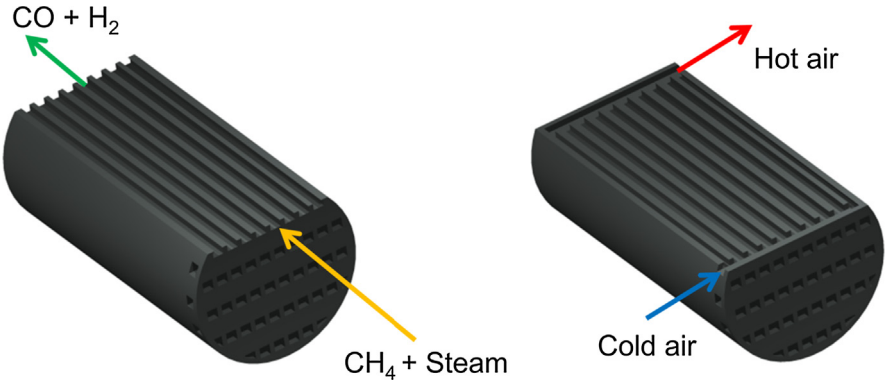

Fig. 1. CONTISOL conceptual monolithic receiver-reactor with separated gas channels for two flow steams.

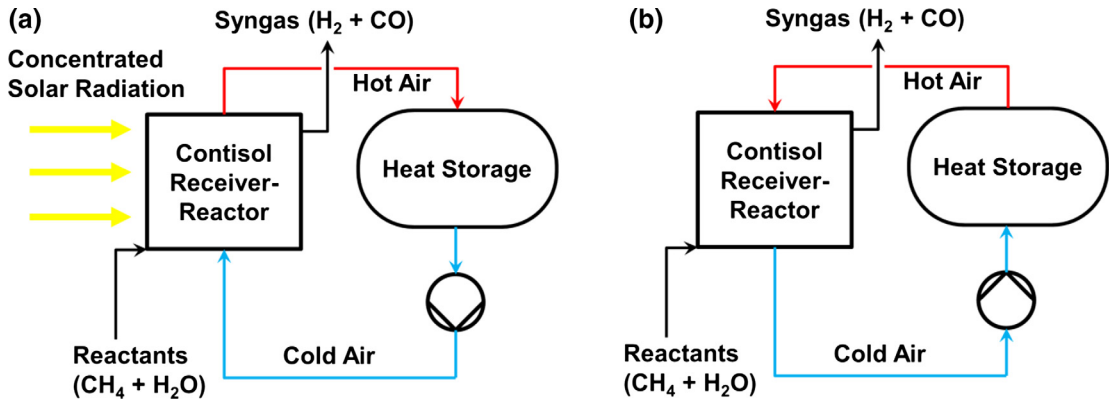

Fig. 2. (a) Daytime operation of the concept, where chemical processing occurs alongside heating of air which is sent to thermal storage. (b) Nighttime operation, where air transfers heat from thermal storage to the receiver-reactor to provide energy for the chemical process.

4. Objectives

To test the concept, a 3 kW-scale prototype reactor has been built. The objective of the prototype is to present a suitable implementation of the concept, identify challenges, and to demonstrate all important modes of operation of the concept. The construction includes the reactor only. Storage is simulated by cooling and venting air heated by the reactor, and using electrical heaters to provide hot air into the reactor. Heat recovery is also simulated by electric heating. Testing of the reactor was done at the DLR high flux solar simulator in Cologne, Germany. The simulator, an array of electric lamps and reflectors, produces a focused beam of light similar to that from a heliostat field, but at much smaller scale. The control of the simulator allows for power levels to be held constant at desired values or for the reactor's response to transients to be tested.

The first primary mode of operation of the reactor is "daytime" operation, where solar energy is absorbed by the monolith and transferred to the gas streams. This mode can be adapted to direct the solar energy to the thermochemical process, air heating, or a combination of the two. The experimental goals include quantifying the thermal transfer from radiative energy to each gas stream at various radiative power levels, with varying flow rates and inlet temperatures of the gases.

Initially, the construction must be validated and thermal performance of the system must be quantified. In order to isolate thermal performance, initial testing was done without reactive gasses, using inert mixtures in each of the two monolith channels. Under varying conditions for solar irradiation and flow rates, the effectiveness of heat transfer to each set of channels, and the amount of energy to each channel is found experimentally. It is desired to determine which process parameters, including the inlet temperatures and flow rates of both channel sets, affect the energy uptake by the two gas streams. These thermal tests in the "daytime" mode are the subject of the current study. Further publications will cover testing of chemical performance and an updated design.

5. Methodology

5.1. Monolith fabrication

As a test of the novel concept, a custom honeycomb monolith was constructed from siliconized silicon carbide (SiSiC). It measures 14.4 cm in diameter, and 20 cm in length. All channels, both straight and side inlet, have a 2 × 2 mm cross section with 0.5 mm thick walls separating the channels. The diameter was selected to fit within an existing reactor housing for the target power level. The diameter is also based on standard silicon carbide extrusion geometry. The smallest available standard channel size for this diameter extrusion was selected to provide the best heat transfer between channels. The monolith, beginning as a porous recrystallized silicon carbide (RSiC) extrusion, was first machined by mechanical sawing to make the connection passages for the side inlet channels. These slots for the side inlets and outlets are two channels, or 4.5 mm, wide by 18 mm long. Then the monolith was siliconized, or infiltrated, with silicon carbide to fill the porosity and achieve dense channel walls in order to avoid gas crossover between channels. Finally, dense silicon carbide strips were cemented across the ends of the side inlet channels using Al_2O_3-Ca_2SiO_4 Aremco Ceramabond™ cement suitable for 1650 °C. These steps are shown in Fig. 3.

5.2. Reactor design

The monolith was mounted in a stainless steel shell with a diameter of 46 cm. A rendering and photographs of the reactor are shown in Fig. 4. The space between the monolith and the reactor shell was filled with Insulfrax® Rohrfaser R lose mineral insulation. One end of the monolith was exposed to irradiation and covered by a quartz window approximately 10 cm from the monolith end. The window is 30 cm in diameter and held by a spring-loaded, water-cooled flange. Side inlets and outlets of the monolith are connected to ports on the reactor shell by internal stainless steel assemblies and hoses, shown in Fig. 4b. The axial channel inlets are open facing the window, and radiation is incident on the channel ends, penetrating into the channels. Gas for these channels is injected by four radial inlets located between the window and monolith. Gasses exit the axial channels through a single ceramic funnel connected to a port on the reactor shell.

5.3. Experimental system

Experiments with the reactor require systems to provide inlet gasses, handle and analyze outlet gasses, and to provide a simulated solar input. The gas management and measurement system is given in Fig. 5. The inlet gasses are supplied through electronically controlled mass flow controllers. The air side is preheated by a 6 kW resistive heater up to 900 °C. Preheating the air simulates the return from a thermal storage system, while preheating the reactants simulates heat recovery from the hot product stream to the cool inlet stream in a heat exchanger. The reactant side is preheated by a 3 kW tube furnace heating the outside of a stainless steel tube packed with stainless steel wool through which the reac-

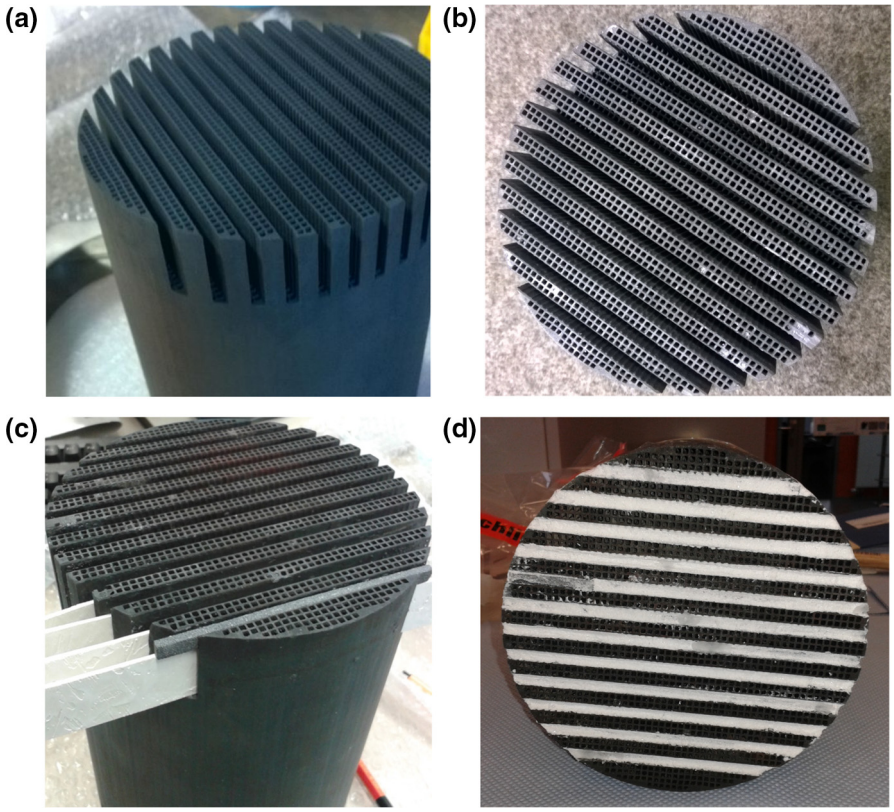

Fig. 3. Fabrication of the receiver reactor monolith. (a) RSiC extrusion with machined slots (b) Siliconized monolith (c) Placing SiC sticks to close side-inlet channels (d) SiC sticks sealed with Al_2O_3-Ca_2SiO_4 cement and fired.

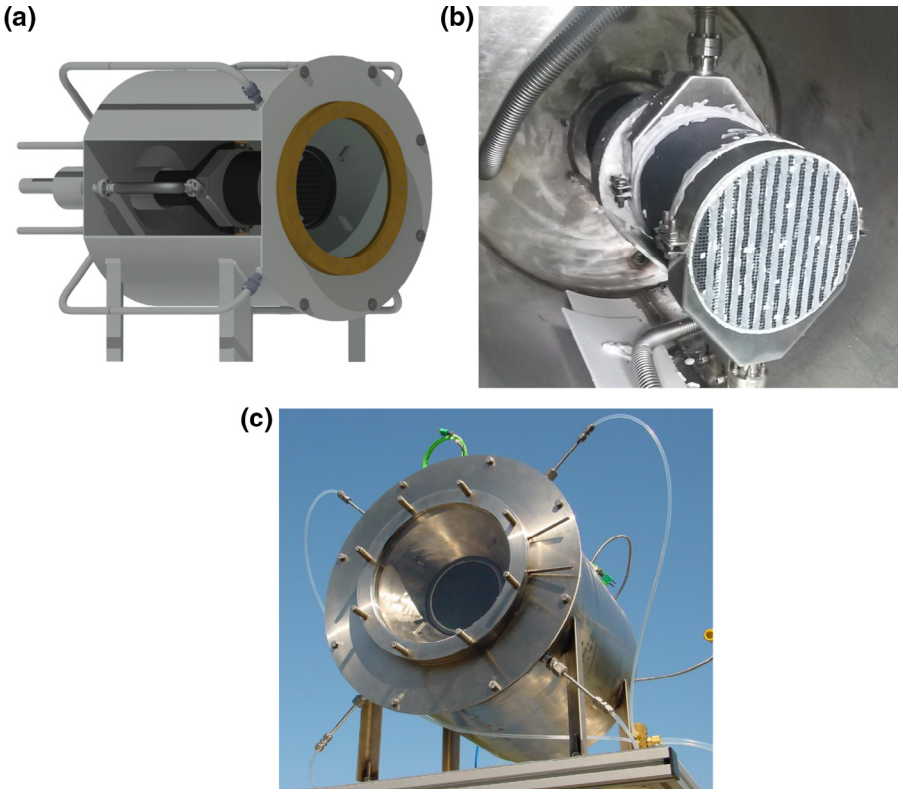

Fig. 4. Construction and assembly of the reactor. (a) Solid model of reactor shell and monolith mounting (b) Monolith mounted with side inlet piping (c) Closed reactor with monolith end exposed and covered by a quartz window.

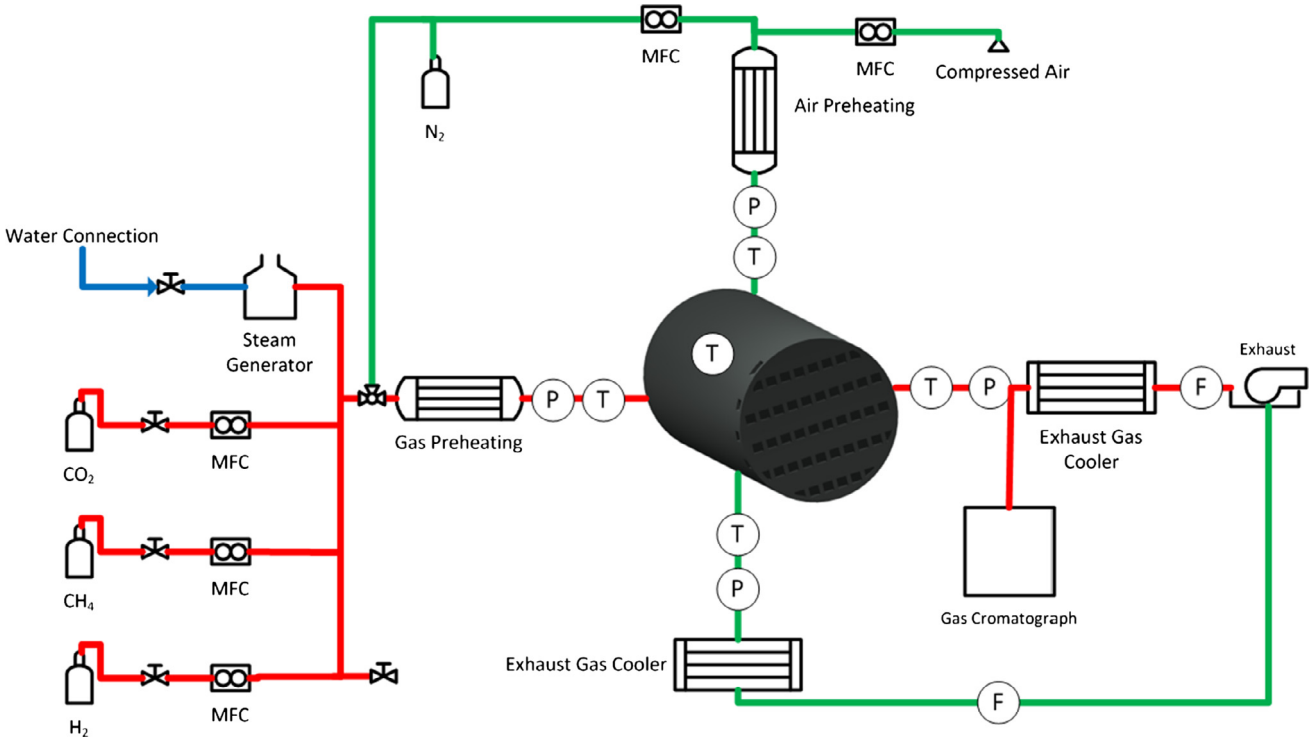

Fig. 5. Diagram of gas management system for experimental demonstration of reactor concept. Circles indicate measurement points for temperature (T), pressure (P) and flow rate (F).

tive gas passes. The design was selected to be compatible with a flow of reactive gases. The reactant preheater is limited to a maximum outlet temperature of 300 °C. Both gas streams are cooled and vented after leaving the reactor. The composition of the reactive gasses was measured by gas cromotragraphy. In future experiments, the mixture of reactants for both steam and dry reforming will be varied. For thermal qualification of the system, nitrogen is routed through the reactant path: the straight channels. This allows the measurement of oxygen in the reactant stream to be used to identify gas cross-over.

Pressures and temperatures of both streams were measured before and after flowing through the monolith. In addition, the monolith was instrumented with 27 thermocouples, with 9 located at each end and at the midpoint. The exact positions of the thermocouples are shown in Fig. 6.

Solar radiation was supplied by DLR's 10-lamp high flux solar simulator [24]. Depending on the monolith temperatures desired, between one and three simulator lamps were used. The focal point was located at the center of the exposed monolith surface. The simulator provided between 1.5 and 4.7 kW of irradiation incident on the monolith. The flux profile of the concentrated irradiation at the absorber surface was measured before testing. A typical flux profile is shown in Fig. 7. The experimental setup and the solar simulator are shown in Fig. 8.

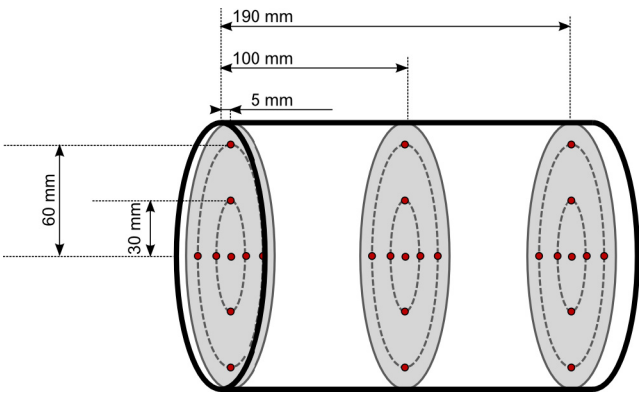

Fig. 6. Position of thermocouples in the monolith. Solar input enters from the left.

5.4. Experimental design

Thermal experiments began with setting a target preheat temperature and flow rate for each set of channels. Gas flow was started before electrical power was applied to either preheater. A PID controller adjusted the air preheater power to match the

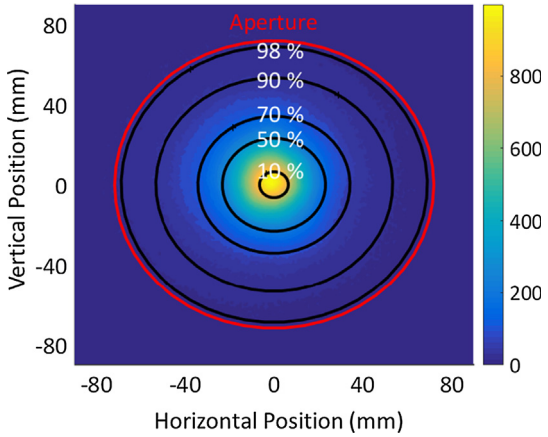

Fig. 7. Flux map of solar simulator at the aperture plane in kW/m^2. The percentage lines mark regions where the total power within the circles meets the corresponding value. Just above 98% of the total power directly irradiates the reactor.

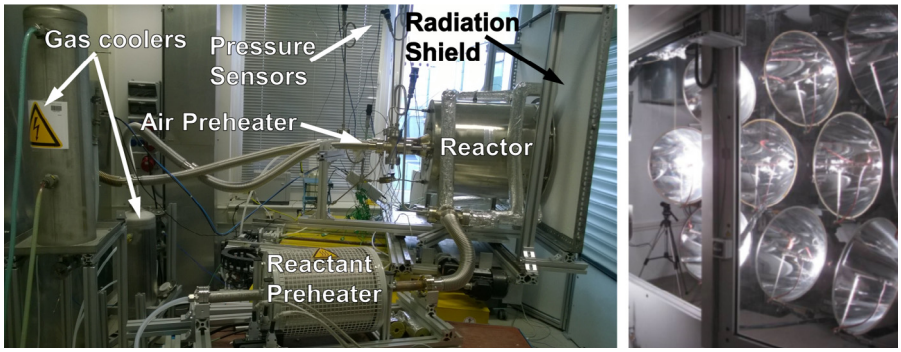

Fig. 8. Experimental setup and DLR high-flux solar simulator.

desired air stream temperature, while the temperature of nitrogen, standing in for the reactive mixture, was approximately controlled by setting the tube furnace power based on a look-up table created in pre-testing. Thermocouples located in the flow streams at the reactor shell measured the temperatures of both flows. When temperatures of the inlet gas streams had stabilized, radiation was applied using the simulator, always beginning with one lamp at the lowest possible current. When the temperature had reached at least 200 °C, additional lamps were powered on corresponding to the desired front temperature of the monolith. Temperatures were allowed to stabilize, which required between twenty minutes and two hours.

During thermal testing, the primary objectives were to ensure that the desired outlet gas temperatures could be reached, and to quantify the heat transfer between the incident radiation and the two gas streams. The heat transfer will primarily depend on the absorber front temperature, the flow rates and the inlet temperatures of the two streams. In total, five variables make up the design space for thermal testing. The flow direction through the monolith will also play a role in heat transfer. However, the most promising orientation was selected for initial testing, which is shown in Fig. 1. Both gas streams enter at the irradiated end of the monolith, helping to reduce the front face temperature for lowered re-radiation losses, and reactants flow through the channels open to irradiation to maximize syngas production.

In order to reduce the amount of required tests to create predictive performance maps of the system, the design of experiments method was applied using a fractional factorial design called D-optimal [25]. The main concept of this process is to not change one factor at a time (OFAT) in successive measurements, but to vary multiple factors simultaneously. The fractional factorial approach allows for testing with only select combinations of parameter values, separated optimally across the design space. This way, a limited number of measurements span a considerably wider scope within the five-dimensional parameter space mentioned above. In our case, applying the D-optimal design required at least 22 parameter variations, while a full factorial design would have required 80. A regression analysis after experimentation leads to a model polynomial which predicts the output (in this case the heat transfer rates) for all combinations of input variables within the limits of the experimental parameter space. In the next step, by analyzing the significance of all terms, only the relevant relations are included in the polynomial. The software Cornerstone® was used for an automated stepwise regression analysis. The criteria for determining which terms to move into or out of the polynomial are the significance levels of all terms. The performance predictions from this method include statistical uncertainty inherent to the regression analysis, in addition to the measurement uncertainty, both of which are quantified in the results.

6. Results

6.1. Sample experimental data

A typical temperature profile of the absorber front and back during one day of testing is shown in Fig. 9(a) and (b). The front side temperatures exhibit a considerably shorter response time to system changes than the back side temperatures. For example, at 9:45 all solar simulator lamps were turned off for a short period of time in order to adjust the system set-up. During this period, the front temperatures decreased by more than 500 °C, while the back temperatures did not exceed a 90 °C drop. Therefore, the back side temperatures were selected as a measure to define steady state

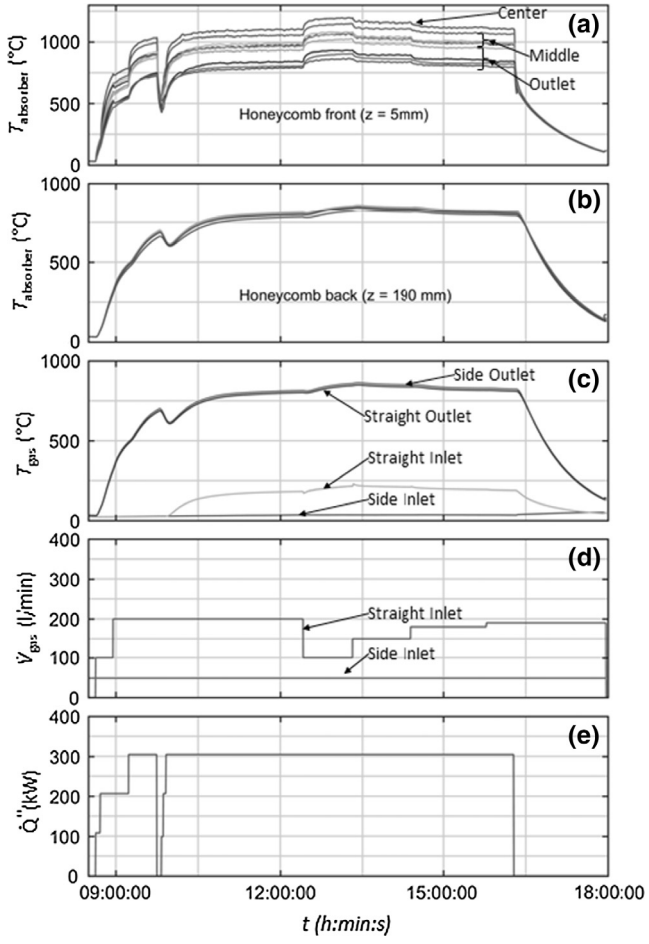

Fig. 9. Measured data during one day of testing.

during the experiments. Whenever all of these temperatures did not change more than 1 K within 10 min, the steady state criterion was fulfilled and the next measurement was taken.

The inlet and outlet gas temperatures, flow rates, and the input power corresponding to the temperature profiles in Fig. 9 (a) and (b) are shown in Fig. 9(c) to (e). Both gas stream outlet temperatures in Fig. 9 reach 850 °C, even during varied flow rates. Though a quite simple result, it is important to the validation of the design efforts to prove that the monolith is capable of heating gasses above the 800 °C necessary to drive the methane reforming reaction. It indicates that the material and designed geometry provide sufficient heat transfer to the gas streams, so that these heat transfer aspects will not prevent this design from succeeding in chemical tests.

Another important observation is that the temperature profile is inhomogeneous in radial direction at the absorber front and becomes more homogeneous towards the back of the absorber. The temperature profiles in the vertical and horizontal directions are shown in Fig. 10. The reason for the inhomogeneous profile is the flux distribution at the absorber front (see Fig. 7), which has much greater flux at the center of the absorber than at the outer edges. In solar tower systems, sophisticated aim point strategies allow for adjusting the flux profile to the needs of the receiver system [26]. Thus, in a large plant the flux profile of the incident radiation would be more homogeneous. As the SiSiC material has a high thermal conductivity, the temperature profile is more homogeneous already at the middle of the absorber (z = 100 mm).

The flux profile is not the only parameter influencing the temperature profile. The position of the side inlet also plays a role. The plots in Fig. 10 reveal that the horizontal temperature profile is rather symmetric while the profile in vertical direction seems to be a superposition of the radiation flux profile effect and another effect reducing the bottom temperatures. This difference between the horizontal and vertical profile is especially pronounced at the front. The asymmetric effect in the vertical temperature profile is caused by the cool gas inlet flow at the bottom. The resulting temperature difference between top and bottom may reach 100 °C or more. A less pronounced temperature difference can still be observed at the central part of the monolith. This effect should be taken into account in a large plant, because the temperature has a strong influence on the chemical conversion. One means to reduce the temperature difference is to adjust the flux profile. Another means could be to apply a custom channel size profile in order adjust the flow resistance in the channels and thus the flow velocity. A lower flow velocity will lead to higher temperatures.

6.2. Design of experiments results

In total, 23 different experimental trials were performed during the test campaign. The set-point conditions, the resulting thermal energy uptake rate of the straight gas stream ($\dot{Q}_{str}$) and the gas stream with side connections ($\dot{Q}_{side}$) are shown in the supplemental material.

The primary measure of performance for the series of thermal tests is the sensible energy gained by the gas streams. In a system with reactions occurring, this sensible energy would be driving the reactions, so it serves as the most appropriate proxy for energy output. The thermal energy uptake was calculated based on flow rate data from mass flow controllers and temperatures taken from thermocouples measuring inlet and outlet gas temperatures for the two channel sets. Heat capacities are assumed constant and taken at 250 °C [27]:

$$\dot{Q}_{side} = \dot{m}_{side} c_{p,side} (T_{out,side} - T_{in,side}) \quad (1)$$

$$\dot{Q}_{straight} = \dot{m}_{straight} c_{p,straight} (T_{out,straight} - T_{in,straight}) \quad (2)$$

The maximum value of $\dot{Q}_{side}$ during performed experiments was 2.16 kW, while the maximum value of $\dot{Q}_{straight}$ was 3.16 kW. In a preliminary examination of the data, energy uptake was highest for high values of flow rates, as expected. Greater energy uptake rates in the straight channels, where less thermal resistance exists between the radiation absorption and the gas, are also expected. The key input variables, temperature and volumetric flow rates, are nondimensionalized for presentation of statistical fits according to the maximum value used during experimentation.

$$T^*_{str} = \frac{T_{str}}{200\,^\circ\mathrm{C}}, \quad T^*_{side} = \frac{T_{side}}{750\,^\circ\mathrm{C}}, \quad T^*_{front} = \frac{T_{front}}{1000\,^\circ\mathrm{C}} \quad (3)$$

$$\dot{V}^*_{str} = \frac{\dot{V}_{str}}{120\mathrm{l\,min^{-1}}}, \quad \dot{V}^*_{side} = \frac{\dot{V}_{side}}{200\,\mathrm{l\,min^{-1}}} \quad (4)$$

An interaction model was used to fit the two data sets: for the side and straight channel power uptakes. The statistical fit considered potential terms that were linear with respect to one variable and second order interaction terms based on the product of two input variables, for a total of 15 potential terms in each fit. Starting

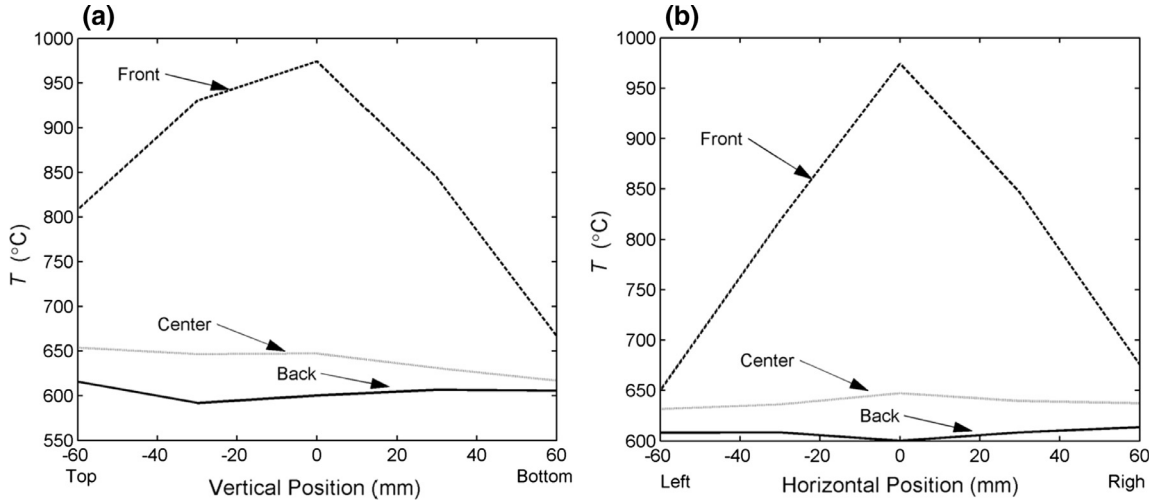

Fig. 10. Temperature distribution in the monolith in the (a) vertical direction and (b) horizontal direction, shown at the axis of symmetry for both directions.

by a least squares fit with the full 15 terms, the significance of each term, or the likelihood of a random interaction of this term producing the observed results, is produced. The significance thresholds to move a term into or out of the polynomial were 0.025 and 0.05. Any terms below the significance threshold are moved out, and then it is tested for each term whether moving it into the fit would result in a significant term. The fit it iteratively adjusted until convergence occurs. The statistical analysis of the data resulted in two formulas describing the parameter set's influence on $\dot{Q}_{side}$ and $\dot{Q}_{str}$, which respectively contain 12 and 10 of the possible 15 terms:

$$\begin{aligned}\dot{Q}_{side} = (&6.234T^*_{str} + 7.950T^*_{side} + 0.5752\dot{V}^*_{str} - 3.954\dot{V}^*_{side} \\ &+ 6.374T^*_{front} - 0.007862T^*_{str}\dot{V}^*_{str} - 0.03613T^*_{front}T^*_{str} \\ &- 0.007095T^*_{side}\dot{V}^*_{str} - 0.03651T^*_{side}\dot{V}^*_{side} \\ &- 0.01674T^*_{front}T^*_{side} + 0.01202\dot{V}^*_{side}\dot{V}^*_{str} \\ &+ 0.06014T^*_{front}\dot{V}^*_{side} - 7.327)\text{kW} \end{aligned} \quad (5)$$

$$\begin{aligned}\dot{Q}_{str} = (&0.5488T^*_{str} + 0.1653T^*_{side} - 0.02258\dot{V}^*_{str} + 0.05912\dot{V}^*_{side} \\ &+ 0.3535T^*_{front} - 0.007680T^*_{str}\dot{V}^*_{srt} - 0.00059T^*_{str}\dot{V}^*_{side} \\ &- 0.002525T^*_{front}T^*_{str} - 0.001108T^*_{side}\dot{V}^*_{str} \\ &+ 0.023027T^*_{front}\dot{V}^*_{str} - 0.6899)\text{kW} \end{aligned} \quad (6)$$

The corresponding adjusted R-squared values are 0.9988 and 0.9999 for $\dot{Q}_{side}$ and $\dot{Q}_{str}$. Thus, the statistical quality of the results is excellent. With Eqs. (5) and (6), it is possible to determine the values of $\dot{Q}$ for the complete parameter space which is spanned by the input values listed in the supplemental materials. Because all parameters have been normalized to a [0,1] scale, it is possible to compare some general influence by the relative coefficient values on input parameters. For example, in Eq. (5), the coefficients indicate a much stronger dependence on $\dot{V}^*_{side}$ than on $\dot{V}^*_{str}$, as would be expected for the value of $\dot{Q}_{side}$. The dependence of the heat transfer rates on the different input parameters is presented in Figs. 11 and 12. On the x-axis in each graph, only one parameter is varied, and the remaining four parameters are fixed at a constant value. The constant values are listed in Table 1. Uncertainties from the statistical fit were much narrower for the power taken up by the straight channels: ±0.005 kW at baseline values and ±0.02 kW maximum, compared to uncertainties for the side channels of ±0.08 kW baseline and ±0.35 kW maximum. Measurement uncertainty was ±0.11 kW for the straight channels and ± 0.082 kW for the side channels at baseline values, similar in magnitude to statistical uncertainty.

The shaded bands in Figs. 11 and 12 represent the statistical 95%-confidence interval. In Fig. 12, the bands are plotted, but are extremely small.

The results give an understanding of the behavior of the system, which is generally intuitive. Greater absorber temperature, which requires greater radiative power input for an otherwise fixed set of parameters, leads to greater energy uptake by both gas streams. Increased flow rates and decreased gas inlet temperature led to higher energy uptake by that gas stream, and each stream is more affected by its own parameters than the parameters of the other stream. With these results, the thermal behavior of the receiver-reactor is characterized and can be used for future planning of experiments, including chemical processing experiments. Although the results are rather trivial from a qualitative perspective, a quantitative performance map is necessary for real-time control of the system and optimized operation.

6.3. Design limitations

Testing revealed several limitations to the current design that prevented continuation of the initial test plan. Most notable was leakage between the reactant stream and the air stream. Leakage occurred by two mechanisms. The first was incomplete sealing of the connections between the honeycomb and the metal gas handling system that supplied air to the side inlets. Though the metal assembly was connected tightly with a gasket and sealant paste, under slight pressure leakage was observed between the metal and gasket, as seen in Fig. 13a. We attribute this leakage to the difficulty of connecting the metal and ceramic components, as the sealing pressure must not exceed structural strength of the ceramic. We expect that this challenge is solvable with modifications to the assembly design, and proper cementing of the metal components to the monolith, something we sought to avoid in order to demonstrate component interchangeability. The more challenging source of leakage was within the monolith. Testing of the monolith revealed that that the infiltration step did not create sufficient density within internal walls to prevent gases from crossing between channels. The supporting observations included summing gas flows in and out of the channel sets during high temperature testing, as well as testing at ambient temperature where the monolith, submerged under water, was shown to produce a gas outflow from several channels with a sealed inlet to one channel. During some

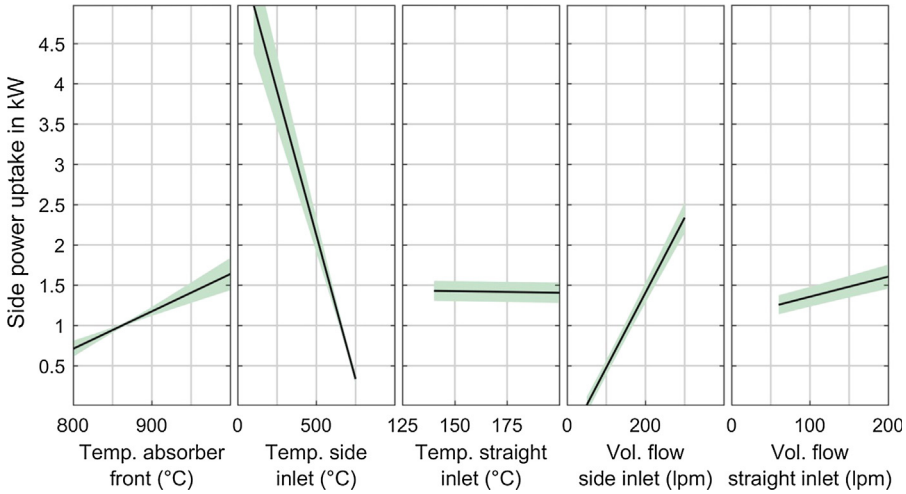

Fig. 11. Influence of input parameters on $\dot{Q}_{side}$.

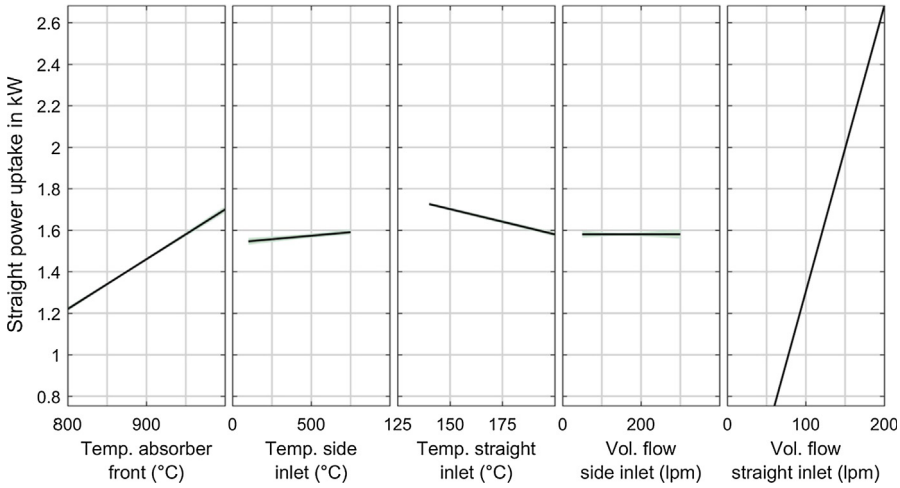

Fig. 12. Influence of input parameters on $\dot{Q}_{str}$.

Table 1
Baseline values of parameters for Figs. 11 and 12.

Parameter	Symbol	Fixed value
Temperature absorber front	T_{front}	950 °C
Temperature side inlet	T_{side}	600 °C
Temperature straight inlet	T_{str}	200 °C
Volumetric flow rate side inlet	$\dot{V}_{str}$	200 L/min
Volumetric flow rate straight inlet	$\dot{V}_{str}$	120 L/min

experiments, a difference in flow rates between the two channel sets forced a significant amount of gas from one set of channels to the other within the monolith, as shown in Fig. 13b where the side outlet flow varies despite a constant side inlet. For this reason, without further study into the fabrication technique, we do not recommend this type of SiSiC construction for structures that must contain gas-impermeable barriers.

An additional challenge was the necessary time to reach steady state for the test receiver/reactor, generally between 30 min and 2 h. In implementation with natural sunlight, this time matches well with morning transients, but it is a much larger time scale than potential changes to gas inlet temperatures and flow rates. In order to test dynamic response of the reaction, a faster responding system would be desired.

6.4. Future improvements and planned work

The limitations of leakage and response time can be addressed by developing a monolith with lower overall volume, and a constructing it of denser material. To accomplish these goals, it was selected to use selective laser melting to 3D print a test monolith section sample from Inconel 618. The channel design follows the general description given for the CONTISOL concept, with all channels running axially but in two separated groups. The new monolith also has 2 mm by 2 mm channels, and rows of channels alternate between the two gas streams, unlike the ceramic monolith where groups of two rows alternated. The sample production is shown in Fig. 14a. Gas tightness tests performed with the sample proved that gas crossover between neighboring channels is negligible at pressure differences up to 1 bar. One issue which arose from the use of a metal monolith was the ability of the Inconel to be coated with catalyst. The as-produced material proved too smooth

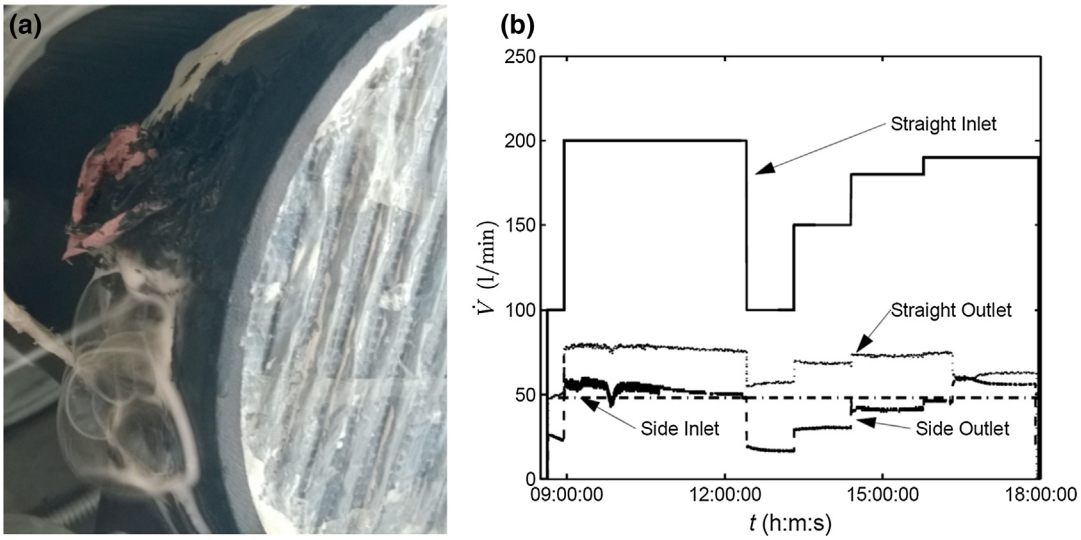

Fig. 13. (a) Leakage observed between the metal gas handling assembly and the SiSiC monolith, and (b) inlet and outlet flow rates, showing the side outlet variation despite a constant side inlet flow.

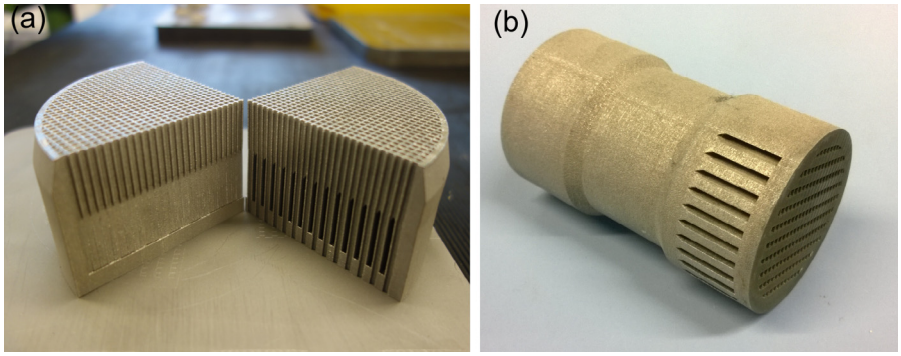

Fig. 14. New metal monolith made with selective laser melting of Inconel 618. (a) Showing a production test sample, and (b) showing the newly created prototype monolith.

for catalyst to adhere. A custom acid etching procedure was performed and led to sufficient surface roughness for catalyst to adhere to the metal surface. The success in solving these problems led to the production of a prototype scale Inconel monolith, shown in Fig. 14b as produced from the laser melting process. The new monolith is 5.4 cm in diameter and 10 cm in length. Additional experiments with this prototype to connect gas inlet manifolds proved successful as well. The same concept of a circular clamped manifold was used, but the strength of Inconel allows for much greater clamping force of the gas connection hardware. Preliminary cold testing resulted in no measurable leakage between the two gas streams for the target flow rates. Based on these preliminary tests, we recommend this type of high temperature alloy monolith for applications up to 1200 C. Future work at DLR will include replacement of the silicon carbide monolith with the Inconel version, a reevaluation of thermal performance, and finally, demonstration of both daytime and nighttime methane reforming following the original concept idea.

7. Conclusions and recommendations

The concept described above provides several key advantages over prior solar methane reforming reactors; advantages which are expected to apply to other chemical processes as well. By varying the flow of air, and reversing the air flow to bring energy from thermal storage, a constant stream of chemical fuel can be produced during times of varying solar input and even at night. The system is compact but, due to high heat transfer area, the tested prototype achieved all target temperatures. A key to controlling the system is a suitable thermal performance map. A designed set of experiments and regression analysis allowed for a performance map to be constructed with a limited number of experiments, greatly increasing the utility of the experiments that were run. The controllability and compactness of this system should be applied to other thermochemical processes in the future, but only after limitations of gas-tightness and transient response are addressed.

Acknowledgements

The presented work has been funded by the German Ministry of Education and Research (BMBF) through contract number 03SF0468. CONTISOL is a cooperation between the German Aerospace Center (DLR) funded by BMBF and the Aerosol & Particle Technology Laboratory (APTL) of CERTH-CPERI in Thessaloniki, Greece, funded under the Greek General Secretariat for Research and Technology (GSRT).

Appendix A. Supplementary material

Supplementary data associated with this article can be found, in the online version, at http://dx.doi.org/10.1016/j.applthermaleng.2017.08.001.

References

[1] Nicolas Piatkowski, Christian Wieckert, Alan W. Weimer, Aldo Steinfeld, Solar-driven gasification of carbonaceous feedstock—a review, Energy Environ. Sci. (2011).
[2] United States office of energy efficiency and renewable energy. "Natural Gas Reforming." <http://energy.gov/eere/fuelcells/natural-gas-reforming> (accessed 06.09.2014).
[3] Hartstein, Arthur, Hydrogen production from natural gas, Hydrogen Coordination Meeting (02.06.2003).
[4] Coffari, Paolucci, D'Alessio, Piccirilli, Tiberio, De Maria, Thermochemical conversion of solar energy by steam reforming of methane, Energy 11 (1986) 805–810.
[5] M.E. Dry, High quality diesel via the fischer-Tripsch process – a review, J. Chem. Technol. Biotechnol. 77 (2002) 43–50.
[6] T.A. Chubb, Characteristics of CO2–CH4 reforming-methanation cycle relevant to the Solchem thermochemical power system, Sol. Energy 24 (1980) 341–345.
[7] Buck, Miur, Hogan, Carbon dioxide reforming of methane in a solar volumetric receiver/reactor: the CAESAR project, Sol. Energy Mater. 24 (1991) 449–463.
[8] Kodama, Shimizu, Satoh, Nakata, Shimizu, Stepwise production of CO-rich syngas and hydrogen via solar methane reforming by using a Ni(II)–ferrite redox system, Sol. Energy 73 (2002) 363–374.
[9] Weimer, Dahl, Bingham, Lewandowski, Bruetsch, Steinfeld, Dry reforming of methane using a solar-thermal aerosol flow reactor, Ind. Eng. Chem. Res. 43 (2004) 5489–5495.
[10] C. Agrafiotis, H. von Storch, M. Roeb, C. Sattler, Solar thermal thermal reforming of methane feed stocks for hydrogen and syngas production—a review, Renew. Sustain. Energy Rev. 29 (2014) 656–682.
[11] V. Anikeev, V. Parmon, V. Kirillov, K. Zamaraev, Theoretical and experimental studies of solar catalytic power plants based on reversible reactions with participation of methane and synthesis gas, Int. J. Hydrogen Energy 15 (1990) 275–286.
[12] R. McNaughton, Solar steam reforming using a closed cycle gaseous heat transfer loop, in: Proceedings of 2012 solarPACES, concentrating solar power and chemical energy systems conference Marrakech, Morocco, September 11th–14th, 2012.
[13] R. McNaughton, W. Stein, Improving efficiency of power generation from solar thermal natural gas reforming. In: Proceedings of 15th international solarPACES concentrating solar power symposium, Berlin, Germany, September 15th–18th; 2009.
[14] M. Epstein, I. Spiewak, A. Segal, I. Levy, D. Lieberman, M. Meri, et al. Solar experiments with a tubular reformer, in: Proceedings of the eighth international symposium on solar thermal concentrating technologies, Köln, Germany, 1996, pp. 1209–1229.
[15] M. Böhmer, U. Langnickel, M. Sanchez, Solar steam reforming of methane, Sol. Energy Mater. 24 (1991) 441–448.
[16] S.A. Paripatyadar, J.T. Richardson, Cyclic performance of a sodium heat pipe solar reformer, Sol. Energy 41 (1988) 475–485.
[17] R.B. Diver, J.D. Fish, R. Levitan, M. Levy, E. Meirovitch, H. Rosin, et al., Solar test of an integrated sodium reflux heat pipe receiver/reactor for thermochemical energy transport, Sol. Energy 48 (1992) 21–30.
[18] A. Wörner, R. Tamme, CO2 reforming of methane in a solar driven volumetric receiver–reactor, Catal. Today 46 (1998) 165–174.
[19] M. Epstein, Solar Thermal Reforming of Methane, SFERA Winter School, Switzerland, Zürich, 2011.
[20] A. Meier, SolarPaces annual report—Task II solar chemistry research, 2010.

[21] A. Berman, R.K. Karn, M. Epstein, Steam reforming of methane on a Ru/Al2O3 catalyst promoted with Mn oxides for solar hydrogen production, Green Chem. 9 (2007) 626–631.
[22] Kodama, Isobe, Kondoh, Yamaguchi, Shimizu, Ni/ceramic/molten-salt composite catalyst with high-temperature thermal storage for use in solar reforming processes, Energy 29 (2004) 895–903.
[23] Romero, Marcos, Osuna, Fernandez, Design and implementation plan of a 10 mw solar tower power plant based on volumetric-air technology in Seville (Spain), in: Proceedings of the Solar 2000, Madison, WI, USA, 2000.
[24] Gerd Dibowski, Andreas Neumann, Peter Rietbrock, Christian Willsch, Jan-Peter Säck, Karl-Heinz Funken. Der neue Hochleistungsstrahler des DLR - Grundlagen, Technik, Anwendung. Kurzfassungen der Vorträge und Poster. 10. Kölner Sonnenkolloquium, 21, Juni 2007, Köln.
[25] Heath Rushing, Andrew Karl, James Wisnowski, Design and analysis of experiments by Douglas Montgomery: a supplement for using JMP(R), SAS Institute Inc., Cary, North Carolina, USA, 2013.
[26] S.M. Besarati, D.Y. Goswami, E.K. Stefanakos, Optimal heliostat aiming strategy for uniform distribution of heat flux on the receiver of a solar power tower plant, Energy Conserv. Manage. 84 (2014) 234–243.
[27] I. Barin, Thermochemical Data of Pure Substances, Weinheim, Wiley-VCH, 1995.